Dakar Niño under global warming investigated by a high-resolution regionally coupled model

Shunya Koseki[1], Rubén Vázquez[2,3], William Cabos[2], Claudia Gutiérrez[2], Dmitry V. Sein[4,5] Marie-Lou Bachèlery[1]

[1]Geophysical Institute, University of Bergen / Bjerknes Centre for Climate Research, Bergen, 5007, Norway
[2]Departamento de Física y Matemátics, Universidad de Alcalá, Alcalá de Henares, 28805, Spain
[3]Instituto Universitario de Investigación Marina (INMAR), Universidad de Cádiz, Cádiz, 11510, Spain
[4]Alfred-Wegener Institute for Polar and Marine Research, Bremerhaven, 27570, Germany
[5]Shirshov Institute of Oceanography, Russian Academy of Science, Moscow, 117218, Russia

Correspondence to: Shunya Koseki (Shunya.Koseki@uib.no)

Abstract. In this study, we investigated the interannual variability of sea surface temperature (SST) along the northwest African coast, focusing on the strong Dakar Niño and Niña events, and their potential alterations under the RCP8.5 emission scenario of global warming using a high-resolution regional coupled model. Our model accurately reproduces the SST seasonal cycle along the northwest African coast and its interannual variability in terms of amplitude, timing, and position of the maximum variability. Comparing the Dakar Niño variability between the 1980-2010 and 2069-2099 periods, we found that its variability intensifies under a warmer climate without changing its location and timing. The intensification is more pronounced during Dakar Niñas (cold SST events) than during Niños (warm SST events) and the ocean temperature variability is connected more deeply with the Dakar Niño variability (vertical motion is more deeply correlated with Dakar Niño variability). The increase of Dakar Niño variability can be explained by the larger variability in meridional wind stresses, which is likely to be amplified in the future by enhanced land-sea thermal contrast and associated sea-level pressure anomalies elongated from the Iberian-Mediterranean area. A heat budget analysis suggests that the horizontal advection anomaly is more explainable for Dakar Niño/Niña in the present climate. However, the future intensification of the Dakar Niño/Niña can be almost identically contributed by the horizontal and vertical advection anomaly that can be intensified by the meridional wind variability.

1 Introduction

From a climatological aspect, the Senegal-Mauritania Frontal Zone (SMFZ, around 9°N-14°N and 20°W-16°W) is one of the most pronounced oceanic frontal zones generated along the eastern boundary current system (Oettil et al., 2021). Here the cold waters of southward Canary Current and Senegal-Mauritania Upwelling System ((Barton et al., 1998; Perez-Hernandez et al., 2013; Vazquez et al., 2022) meet relatively warm tropical waters resulting in a steep sea surface temperature (SST) gradient ((Koseki et al., 2019; Ndoye et al., 2014; Sylla et al., 2019). The northern end of the SMFZ is around 19°N where the Canary Current joints with the north equatorial Current (e.g., (Santana-Falcon et al., 2020) around Cape Blanc (e.g., (Pastor et al., 2008). The Canary upwelling system is tightly connected with the equatorward alongshore wind associated with

the Azores anti-cyclone (e.g., (Davis et al., 1997) and highly dependent on the latitudinal migration of the Intertropical Convergence Zone (ITCZ, (Sylla et al., 2019). Related to the enriched nutrients from the ocean subsurface, the SMFZ and Canary upwelling region also feature an active marine ecosystem (e.g., (Aristegui et al., 2009; Gomez-Letona et al., 2017) and consequently, play an important role in local and regional fisheries such as sardinella from the northwestern Africa to the Iberian coasts in the north tropical-to-subtropical Atlantic (e.g., (Arrasate-Lopez et al., 2012; Becognee et al., 2006; Ndoye et al., 2014).

Apart from these climatological mean-state features, the SMFZ shows intense interannual variability in SST, and extreme events of SST warm anomalies are called Dakar Niño ((Oettli et al., 2016). Principally, Dakar Niño is driven by the local wind anomaly and it peaks between March and April according to (Oettli et al., 2016). A similar mode of SST variability is found in the southeastern tropical Atlantic, which is Benguela Niño ((Bachelery et al., 2020; Koungue et al., 2021; Koungue et al., 2019; Rouault et al., 2018). There, the interannual variability is not only driven by local wind fluctuations, but is also strongly linked to western equatorial winds that trigger the propagation of equatorial Kelvin waves and coastal trapped waves off the African coast (Bachelery et al., 2020; Koungue et al., 2021; Koungue et al., 2019; Rouault et al., 2018) . In spite of that, the inter-annual SST variability in the Dakar system has a major influence on marine ecosystems. For instance, (Lopez-Parages et al., 2020) showed that the distribution of round sardinella tends to be modified following the Dakar-Niño-like pattern initialized by El Niño variability in the tropical Pacific.

For sustainable development, including the fisheries sector, the understanding of climate variability under global warming draws more attention not only from the scientific community, but also from societies, stakeholders, and governments. Climate projections from Earth System Model (ESM), such as the Coupled Model Intercomparison Project Phase6 (CMIP6, (Eyring et al., 2016), are one of the most common tools to investigate future climate change. These ESMs are state-of-the-art models that have been improved in many aspects for the simulation of the climate system and their use for climate prediction (e.g., (Bracegirdle et al., 2020; Choudhury et al., 2022; Priestley et al., 2020). However, model biases in the tropical Atlantic climate are a long-standing issue even in CMIP6 and are very common in most of state-of-the-art ESMs ((Cabos et al., 2017; Richter and Tokinaga, 2020; Richter and Xie, 2008; Voldoire et al., 2019). These biases are one of the main sources of uncertainty in climate projections and therefore, there is a necessity to utilize less systematically-biased ESMs to assess more plausible climate projections. Partially because of model errors mentioned above and relatively recent discovery of Dakar Niño (the first paper on this topic is (Oettli et al., 2016), there are few studies on how the Dakar Niño variability would evolve under global warming while surveys on the equatorial Atlantic variability have been reported recently ((Crespo et al., 2022; Yang et al., 2022).

There are several methodologies to alleviate model errors that have been proposed in the previous studies including the implementation of better parameterization (e.g., (Deppenmeier et al., 2020), heat and/or momentum flux correction/anomaly coupling (e.g., (Dippe et al., 2018; Toniazzo and Koseki, 2018; Voldoire et al., 2019), and interactive model ensembles (e.g., (Shen et al., 2016); Counillon et al., 2023; Schevenhoven et al., 2023). Apart from these methodologies, resolution refinement is also beneficial to improve the model performance in the tropical Atlantic (e.g., (De La Vara et al.,

2020). (Sylla et al., 2022) by assessing the archives of High Resolution Model Intercomparison Project (HighResMIP, (Haarsma et al., 2016), stressed the limited benefits of model refinement to improve the Canary Current upwelling system. On the other hand, (Vazquez et al., 2022) suggest that a high-resolution (mesoscale eddy-permitting scale) regional coupled model is able to represent the Canary Current upwelling systems and surface wind field.

70   This study, therefore, aims to unveil how the Dakar Niño variability would change in the future climate by adapting the reliable high-resolution regional coupled model used in (Vazquez et al., 2022). This paper is structured as follows: Section 2 gives details on the regional coupled model, the experimental setup, and the reanalysis data. We will describe results of model simulations with brief evaluation comparing with reanalysis data in Section 3. Finally, we will give discussions on the results and summary of this study.

75 **2 High-resolution regional coupled model**

   The regionally-coupled model ROM (e.g., (Sein et al., 2020; Sein et al., 2015) configurations used in this study is the same as in Vazquez et al. (2022). It consists of a regional atmospheric component, limited-area Regional Model (REMO, e.g., (Jacob, 2001) and global oceanic component, Max-Planck Institute Ocean Model (MPIOM, e.g., (Jungclaus et al., 2013; Marsland et al., 2003). REMO has 25km horizontal resolution with 27 hybrid vertical levels. MPIOM adapts an orthogonal

80 curvilinear horizontal grid system with shifted poles allowing to refine the focused region while a global domain can be maintained (for more details, see (Sein et al., 2015). In our setting, MPIOM has 5 to 10km of horizontal resolution around the Iberian Peninsula and Cape Ghir at 31°N and 10°W upscaling gradually toward 100km in the Southern Ocean. The ROM's configuration domain utilized in this study is given in Fig.1. Air-sea coupling is active between REMO and MPIOM within the red rectangular shown in Fig.1. Outside of the active regional coupling, the MPIOM is forced by prescribed atmospheric

85 forcing. The REMO is laterally forced by those prescribed atmospheric forcing.

   In this study, ROM is integrated from 1950 to 2099 under historical and the Representative Concentration Pathway 8.5 (RCP8.5) forcing where the anthropogenic emission of greenhouse gases increases until the end of the century. The global atmospheric forcing is derived from the low-resolution Max Planck Institute ESM (MPI-ESM-LR, (Block and Mauritsen, 2013; Giorgetta et al., 2013). At detailed evaluation of the ROM configurations for 1950-2005 historical period with respect

90 to observational products and forced by ERA-Interim (Dee et al., 2011) is demonstrated intensively by (Cabos et al., 2020; Cabos et al., 2017; Vazquez et al., 2022). Here, we analyze the data from 1980 to 2010 as present climate conditions and from 2069 to 2099 as future climate change referring to ROM_P and ROM_F, hereafter. For a brief evaluation of the ROM simulation, atmosphere and ocean reanalysis data provided by the European Centre for Medium Range Weather Forecast ERA5 (Hersbach et al., 2020) and ORAS5 (Zuo et al., 2019), during 1980-2010 and the satellite data of European Space Agency (ESA) SST

95 Climate Change Initiative (CCI) product (Good, 2019) during 1981-2010 is used.
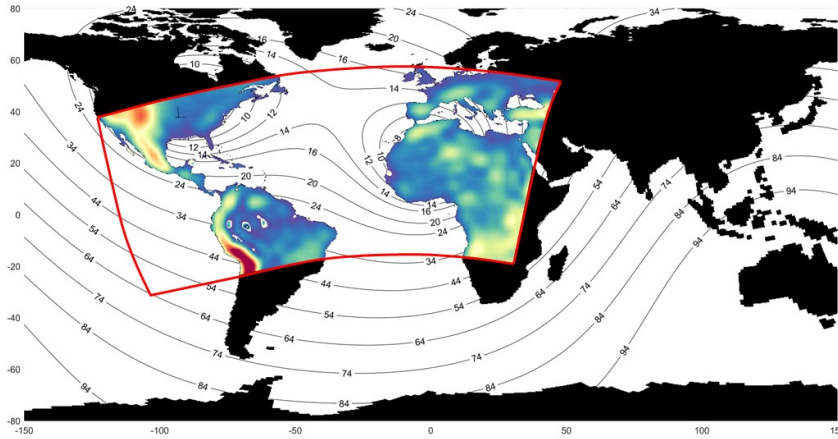
Figure 1: The schematic of the ROM's domain used in this study. REMO is the red-squared domain. The numbers denote the resolution of MPI-OM. The shade show the topography height.

3. Results

3.1 Climatology and interannual variability

First, we assess the SMFZ seasonal cycle and its interannual variability as shown in Fig.2. The results show a clear seasonal cycle displacement of the SMFZ with the cold water penetrating more southward from February to April and being pushed more northward from August to October (Fig. 2a-d). This seasonal meridional migration of SST front could be associated with the seasonal cycle of the Canary Current and upwelling locational changes (Cropper et al., 2014; Pardo et al., 2011; Sylla et al., 2019) by displacing the surface water masses meridionally. Additionally, during winter to early spring, the Mauritania Current flows down to 14°N. Inversely, associated with the relaxation of the trade winds (e.g., (Lazaro et al., 2005), the Mauritania Current reaches the Cape Blanc (around 20°N) associated with the cessation of upwelling south of this latitude ((Mittelstaedt, 1991). This fact leads to a 2.5-fold increase in northward flow during summer compared to the upwelling season, transporting waters of mainly South Atlantic origin into the SMFZ (Klenz et al., 2018). The steep SST gradient is consistent with the SST seasonal cycle and locates at 10°N-12°N in February to April and 20°N-22°N in August to October. Coinciding with the position of the front, enhanced interannual variability appears in November and persists till May with a maximum peak of 1.2 K at 10°N-12°N between February and April (Fig. 2e). This period coincides with the preferred season of Dakar Niño/Niña (Oettli et al., 2016). Another moderate peak of variability is found from August to October at 20°N-22°N when the SST gradient reaches its second maximum at the same timing and location. Similar to these patterns of the SMFZ and Dakar Niño, the Angola-Benguela Frontal Zone (ABFZ, e.g, (Colberg and Reason, 2006; Koseki et al., 2019) and Benguela Niño variability is maximized between February to April (e.g., (Aristegui et al., 2009; Bachelery et al., 2020; Koseki and Koungue, 2021; Koungue et al., 2021; Koungue et al., 2019; Rouault et al., 2018). However, there are dissimilarities between the two coastal interannual modes: the SMFZ seasonal displacement is much wider than the ABFZ whose position is almost seasonally fixed (e.g., (Koseki et al., 2019). The ESA SST shows a similar pattern of seasonality of SST, variability and SST gradient (Figs. 2b and f). Compared to the ERA5, the ESA SST is cooler in all months. This could be due to relatively-poor

representation of coastal upwelling in the ERA5 (coarser than ESA) and the fact that ERA5 has a warm bias (Vazquez et al., 2022). Conversely, the SST meridional gradient is much steeper in the ESA than the ERA5 maybe because the ESA has a finer resolution (0.05 degree) than the ERA5 (0.25 degree).

125   The ROM$_P$ simulation can reproduce the SMFZ well as shown in Figs. 2c compared with Fig 2a. At the lower latitude (EQ to 12°N), ROM$_P$ has cold SST biases in a whole year with respect to the ERA5 and ESA. Such cold SST bias can be seen at the higher latitude (18°N to 30°N), but they are moderate (Fig. 2b). According to Vazquez et al. (2023), coupling and higher-resolution SST allow a better representation of the North African Coastal Low Level Jet (Soares et al., 2019), which is a key pattern of the surface wind field along the North African coast. This good representation of the SMFZ is due to the finer

130   resolution to permit meso-scale eddy and filaments in our focus region in contrast to the common Earth system models like CMIP5 ((Vazquez et al., 2022). The SST variability is also realistically represented in ROM$_P$ (Fig. 2g). The variability is maximized during March to April, which is slightly delayed from the observation. However, its amplitude is as strong as the ERA5 and weaker than ESA (Figs. 2e, f and g). The secondary peak during August to October can be well-captured.
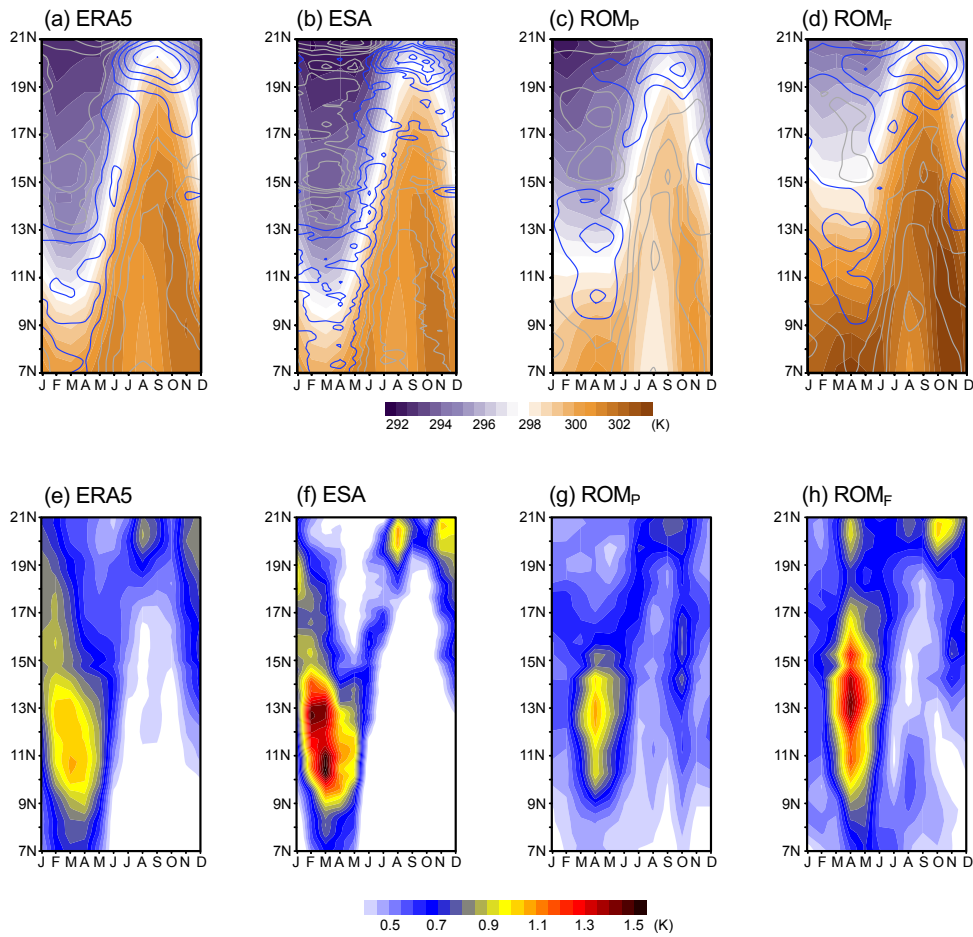
135

Figure 2: Hovmöller plot of (top) sea surface temperature (SST, color) and aboslute value of merdional SST gradient (K/100km, contour, interval is 0.2K/100km). The merdional SST gradient greater than 0.5K/100km is shown by blue. Data are averaged between 21°W and 17°W for ERA5, ESA, ROM$_P$ and ROM$_F$, respectively. (bottom) Same as top panels, but for the standard deviation of detrended SST. Unit is in Kelvin.

140

Under the highest emission scenario, this region experiences significant warming with; the lower latitude warming up by 3°C and higher latitude by 1°C (Fig. 2d). However, the SMFZ location is almost identically between ROM$_P$ and ROM$_F$ (not shown). Interestingly, the Dakar Niño variability is strengthened in both peaks in ROM$_F$ while its timing does not change (Fig. 2h). This response contrasts with the recent studies on the equatorial Atlantic variability reported recently ((Crespo et al.,

145   2022; Yang et al., 2022). The possible mechanism of this reinforcement will be given in the next subsection. To assess the Dakar Niño this study will focus the month of March as it has been determined to be the peak month of the event. Note that despite the slight differences in timing of the SST variability peak compared to observations the simulated March variability is comparably intense (Fig. 2). Therefore, for fairness comparison with observations, we will focus on March throughout the rest of the paper (Fig. S1 gives a time series of SST standard deviation averaged 9°N-14°N).
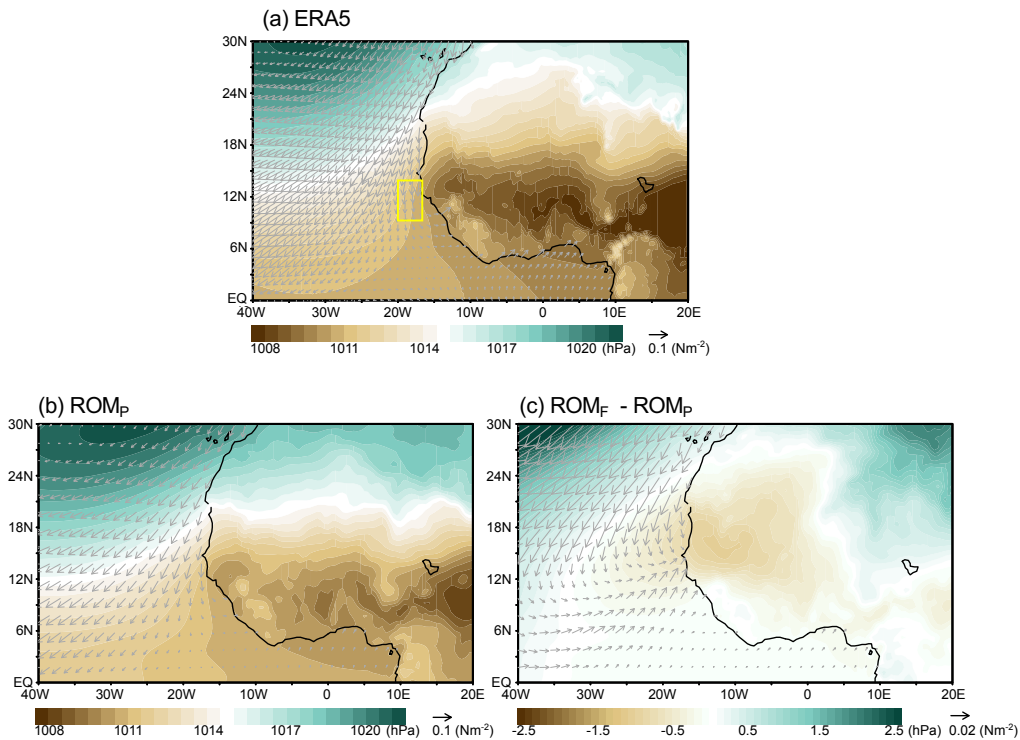
150

Figure 3: March-climatological sea level pressure (SLP in hPa, color) and wind stress (arrows) in (a) ERA5 and (b) ROM$_P$. (c) The difference in SLP and wind streess climatology in March between ROM$_F$ and ROM$_P$. The yellow rectangular denotes the box for Dakar Index.

As shown in Fig. S2, associated with the intense upwelling, the thermocline (20°C isotherm) tilts zonally (shallower in the east) in the reanalysis (Fig. S1a). ROM$_P$ can represent this zonal tilting of thermocline well and the steep vertical gradient

155 is found around 40-60m depth along the coast (Fig. S1b). Under global warming, the thermocline tends to be deeper while the coastal vertical gradient seems stronger than that in ROM_P between 40 and 60m depth (Fig.S1b and c).

In March, the low pressure dominates over western Africa between 6°N and 15°N and the Azores high pressure system sits over the North Atlantic. Due to this contrast of surface pressure, strong southerly wind blows along the western African coast (Fig. 3a). ROM_P simulates this atmospheric circulation realistically while the low pressure over the Sahel is
160 slightly underestimated (Fig. 3b). As shown in Fig. 3c, the continental low pressure is partially deepened, especially, near the coastal area (10°N-24°N and 15°E to 0°E) where the surface temperature at 2m is intensively warmed by 5 degrees in ROM_F (not shown). This strong terrestrial warming can be explained by the desert amplification ((Cook and Vizy, 2015; Zhou, 2016). Corresponding to this deepened low pressure, a cyclonic circulation anomaly is detected around 15°N and 15°W in Fig. 3c. This anomaly pattern is similar to climate projections by CMIP5 ((Sylla et al., 2019). While the upwelling-favourable wind
165 intensifies at higher latitudes (18°N-30°N), onshore wind anomalies form at lower latitude (12°N-15°N).

3.2 Dakar Niño variability

In this subsection, more details of the Dakar Niño modification under the highest emission scenario are investigated employing lag-correlation and composite analyses. These analyses are based on the Dakar Index in March defined as detrended interannual
170 SST anomalies averaged over the 21°W-17°W, 9°N-14°N box ((Oettli et al., 2016). The definition of the Dakar Niño and Niña events relies on the detrended March Dakar Index anomalies that exceed, or fall below, ±1 standard deviation of the Dakar Index. As shown in Fig. 4a, ERA5 counts 7 Dakar Niño and 6 Dakar Niña events over 31 year. In comparison, our ROM simulation, ROM_P and ROM_F, have 7/9 Dakar Niño and 8/6 Dakar Niña events for the present and future climate, respectively. Note that there is no possible consistency in the timing of Dakar Niño and Niña events between ERA5 and ROM_P as the ROM_P
175 simulation is not a historical run. However, the frequency of the events is similar. Under global warming, the frequency of the events seems not strongly influenced (Fig. 4c) while the negative events are stronger than in the present climate (Fig. 4b and c).
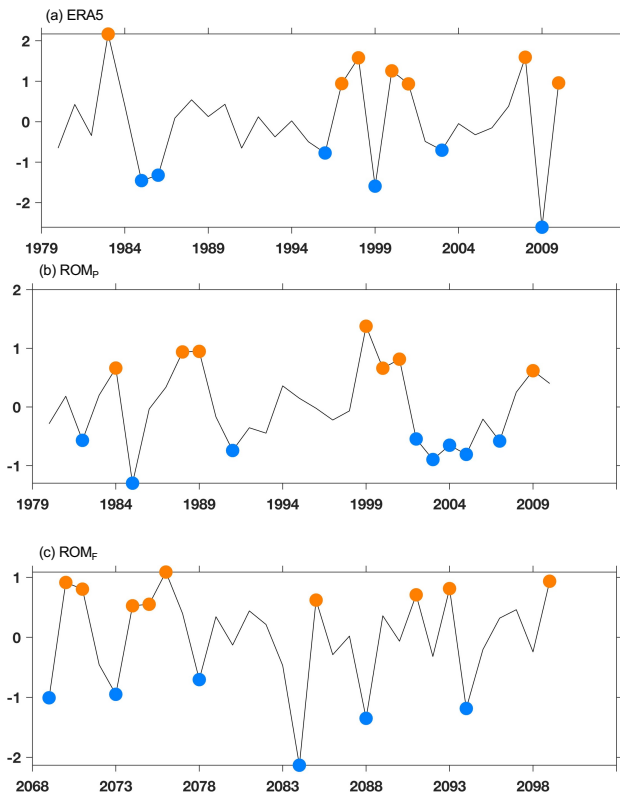
180 **Figure 4**: Time series of Dakar Index (detrended SST averaged 9°N-14°N and 20°W-17°W) for (a) ERA5, (b) ROM_P and (c) ROM_F. The orange and blue dots indicate Dakar Niño and Niña events, respectively.

	Jan (-2)	Feb (-1)	Mar (0)	Apr (+1)	May (+2)
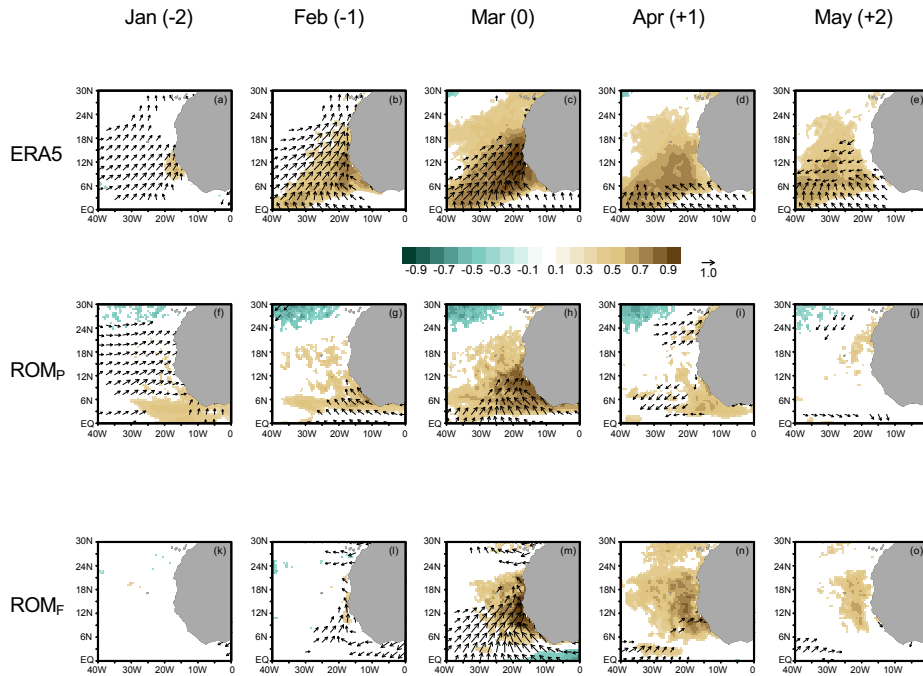
Figure 5: Lag-correlation plots between March Dakar Index (SST over 21°W-17°W, 9°N-14°N) and wind stress (vector) and SST (color). Only the correlation is shown satisfying $p < 0.05$ for (top) ERA5, (middle) ROM$_P$, and (bottom) ROM$_F$, respectively. The vector with significant correlation of zonal or meridional wind component is shown. From the left to the right, the panels show the lag-correlation from January (-2) to May (+2).

In ERA5, positive surface wind correlation (southwesterly) and SST positive correlation are found along the west African coast in January, two months before the peak in March (Fig. 5a). The positive correlation becomes more intense in February to March (Figs.5a and c). In March, the significant correlation of surface wind is relatively localized south of 15°N. After the peak of Dakar Niños, the surface wind correlation is more dominant only around the equator and offshore in April to May (Figs. 5d and e). The positive SST correlation seems to propagate westward, in particular around 6°N to 10°N, in April to May (Figs. 5d and e) and this might be related to Rossby wave propagation inducing the equatorial Atlantic Zonal mode in summer (e.g., (Martin-Rey and Lazar, 2019). In ROM$_P$, the life-cycle of Dakar Niño variability is to some extent simulated realistically: the surface wind correlated in January (Fig. 5f). Positive SST anomalies develop from January to March while the surface wind in February is not well simulated (Figs. 5f-h). The surface wind in March is more locally correlated compared to ERA5 (Figs. 5c and h). After the peak, the positive SST correlation decays, but seems not to propagate westward clearly. However, a signal of westward propagation can be detected at 41m depth (around 6°N) in ROM$_P$ (Fig. S3). Although the evolution of the ROM$_F$-simulated Dakar Niño and correlated surface wind in January and February are not as clear as ROM$_P$ (Figs. 5k and l), the surface wind is correlated more broadly along the coast during March up to 18°N (Fig. 5m) while it is

limited to 12°N in ROM$_P$ (Fig. 5h). After the peak, the positive SST correlation moves westward more clearly like ERA5 even though its phase speed is slower than the ERA5 (Figs. 5n and o). In Fig.S4, climatology of SST and wind stress is given.

205   In ROM$_P$, the significant positive correlation concentrates between the surface and 40m depth and decreases to 100m depth, which is about 0.4 (Fig. 6a). In contrast, the ocean temperature correlates significantly with the Dakar Index more deeply down to 160m depth with 0.5 of correlation in ROM$_F$ (Fig. 6c) indicating that Dakar Niño and Niña events would influence deeper ocean in the future. Comparing the correlation of vertical motion between ROM$_P$ and ROM$_F$, the vertical velocity is correlated more deeply and strongly in ROM$_F$ than ROM$_P$ (Figs. 6b and d): in ROM$_P$, the significantly correlated vertical

210   motion is limited to 40m while the vertical motion in ROM$_F$ is significantly correlated down to 60-80m.
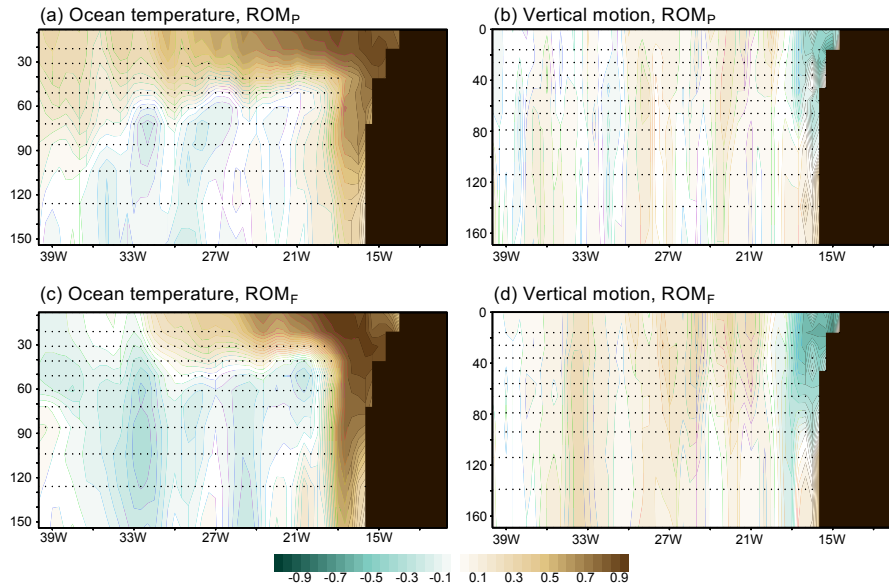
Figure 6: Vertical-longitudinal section of the correlation between the Dakar Index and (left) ocean temperature and (right) vertical motion averaged between 9°N and 14°N for (top) ROM$_P$ and (bottom) ROM$_F$. The dots denote no significance of correlation.

215   Figures 7a-d show the composite of ocean temperature anomalies during Dakar Niño and Niña in ROM$_P$ and ROM$_F$, respectively. Similar to the correlation plot (Fig. 6), the temperature anomalies in ROM$_P$ are large around 40m depth in both Niño and Niña and their magnitudes are almost identical (±1.8K, Figs. 7a and b). Interestingly, the temperature anomalies in ROM$_F$ around 40 m depth are more pronounced during the Dakar Niñas than Niños (Figs. 7c and d). In addition, the temperature anomaly associated with the Dakar Niñas penetrates more deeply in ROM$_F$ than in ROM$_P$ (Figs. 7b and d). That

220   is, the amplification of the variability under global warming is mainly induced by the Dakar Niñas in our simulation. The surface to subsurface ocean is heated up following climate change, but its vertical distribution is heterogeneous (Fig.7e). The ocean surface experiences more efficient warming than the sub-surface. The difference in warming is particularly large around 40m and upper levels where the temperature anomalies due to Dakar Niño/Niña variability and its change is the most intense

(Fig. 7a-d). In addition to the vertical motion change, this strengthened stratification at 40m depth can be implicative for the
225 strengthened Dakar Niño/Niña variability.
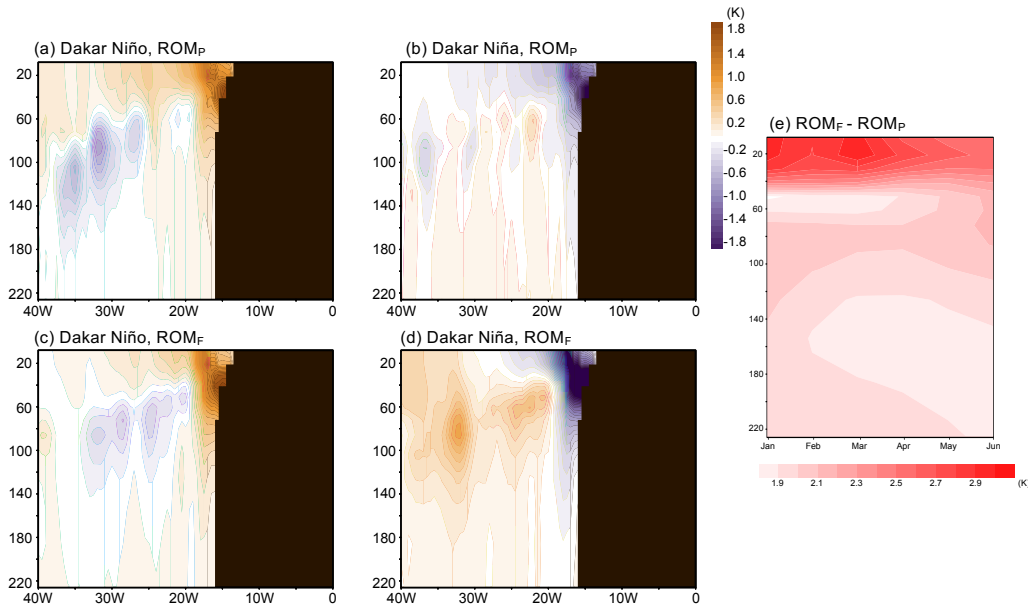
Figure 7: (a)-(d) Composite vertical-longitudal section of the temperature anomalies (K) for Dakar Niño/Niña in ROM$_P$ and ROM$_F$ in March. (e) Vertical-temporal section of the monthly climatological ocean temperature difference between ROM$_F$ and ROM$_P$ averaged over 9°N-
230 14°N and 20°W-16°W.

4. Discussion and Summary

4.1 Why is the Dakar Niño/Niña variability amplified?

The simulations of the high-resolution regionally coupled model, ROM have shown that the Dakar Niño/Niña
235 variability in March will be increased under global warming, especially for the Dakar Niñas. According to (Oettli et al., 2016), the Dakar Niño is driven mainly by changes in alongshore local surface wind and the surface wind changes are investigated in more detail here.

The standard deviation of meridional wind stress anomalies is given in Fig. 8. In the observation, the high variability associated with the Azores high-pressure system (e.g., (Davis et al., 1997) is found between 24°N and 30°N (Fig. 8a). Apart
240 from that, the meridional wind variability is relatively strong along the northwestern African coast down to 9°N as well. ROM$_P$, basically, is able to capture the spatial pattern of meridional wind variability: the coastal largest variability locates around 20°N (Fig. 8b) while the variability around 12°N and 20°W is somewhat overestimated resulting in forming two cores of high variability (in the observation, the second core around 12°N is much smaller and it is located more offshore as shown in Fig. 8a). Under global warming (Fig. 8c), the coastal wind variability is increased while the positions of the two cores are not

245 changed. Inversely, the meridional wind variability over the open ocean between 24°N and 30°N does not seem to change as much as the coastal region (Figs. 8b and c) indicating that the higher wind variability in the future might be more relevant due to local effects around the coastal region.
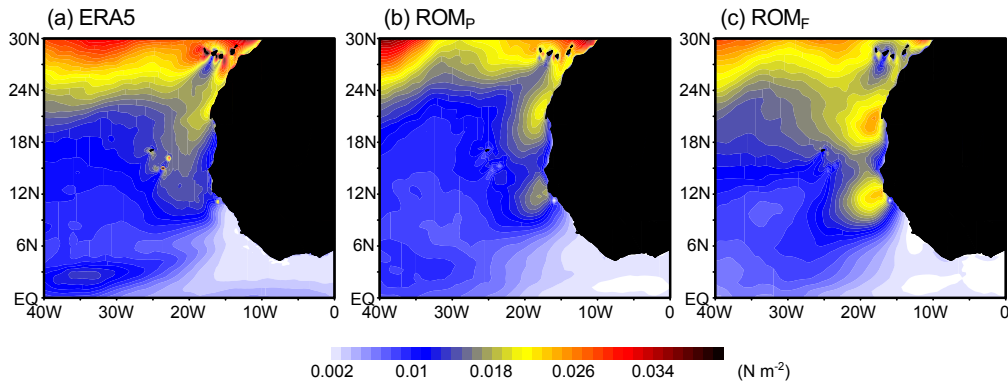
Figure 8: Standard deviation of the meridional wind stress in March for (a) ERA5, (b) ROM$_P$, and (c) ROM$_F$.

A possible explanation for the localized change in the surface wind is the land-sea heat contrast proposed by (Bakun, 1990). According to (Bakun, 1990), in the context of global warming, terrestrial regions will heat up faster and intensely than oceanic region, which will increase the land-sea heat contrast and consequently strengthen the equatorward coastal low-level
255 jet and corresponding upwelling. Figure 9 shows the composite anomalies of 2m temperature during Dakar Niños and Dakar Niñas in ERA5 and ROM simulations. In the ERA5, the 2m temperature anomalies show a land-sea thermal contrast, but the 2m temperature anomalies over the land (signs are opposite to the Dakar Niños/Niñas near the coast) are located far from the western African coast (around 0° to 20°E, Figs. 9a and b). ROM$_P$ can reproduce the terrestrial 2m temperature anomalies realistically in the case of Dakar Niño and Niña although its amplitude is weaker than that in ERA5 (Figs. 9c and d).
260 Conversely, the land-sea thermal contrast associated with the 2m temperature anomalies is more pronounced in ROM$_F$ (Figs. 9c fand f). During the Dakar Niño events, the magnitude of cool anomaly over the continent is almost identical in both present and future climate, but spatially, land-surface temperature anomaly shifts more westward and the zonal surface temperature gradient can be weakened around the coastal region, especially, around 9°N-12°N (Fig. 9b). In the case of the Dakar Niñas, the land surface temperature anomaly shifts more westward similarly to the case of the Dakar Niñas and
265 additionally, its amplitude is much larger in ROM$_F$ than in ROM$_P$ (Figs. 9c and d). This situation can strengthen the zonal thermal contrast and the alongshore (upwelling-favorable) wind can be more effectively generated. In climatology, the ROM simulations show that the desert amplification (e.g., (Cook and Vizy, 2015; Zhou, 2016) is pronounced in the western Africa under RCP8.5 scenario (not shown).
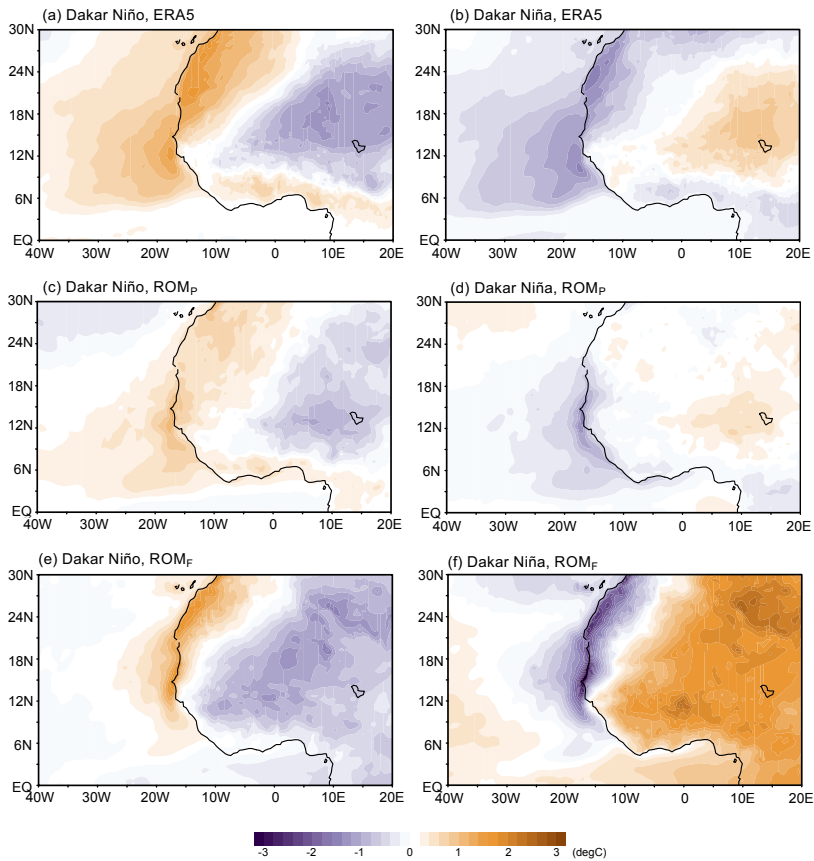
Figure 9: Composite anomalies of the 2m temperature averaged during (left) Dakar Niño/ /(right) Niña events in (top)ERA5, (middle) ROM$_P$, and (bottom) ROM$_F$ in March.

This land-sea thermal contrast anomalies can be also indicated by sea level pressure (SLP) anomalies (Fig.10). In ERA5, the SLP anomalies shows a dipole pattern roughly over the Atlantic Ocean and the continent (Figs. 10a and b). While the SLP anomaly over the Atlantic can be relevant to the Azores high pressure, the SLP anomalies over the Sahara connect to the SLP anomalies over the Mediterranean and the SLP anomaly over the continent appears to be more responsible for creating the SLP zonal gradient along the coast, in particular, case of Dakar Niña (Fig. 2b). The ROM$_P$ can represent this
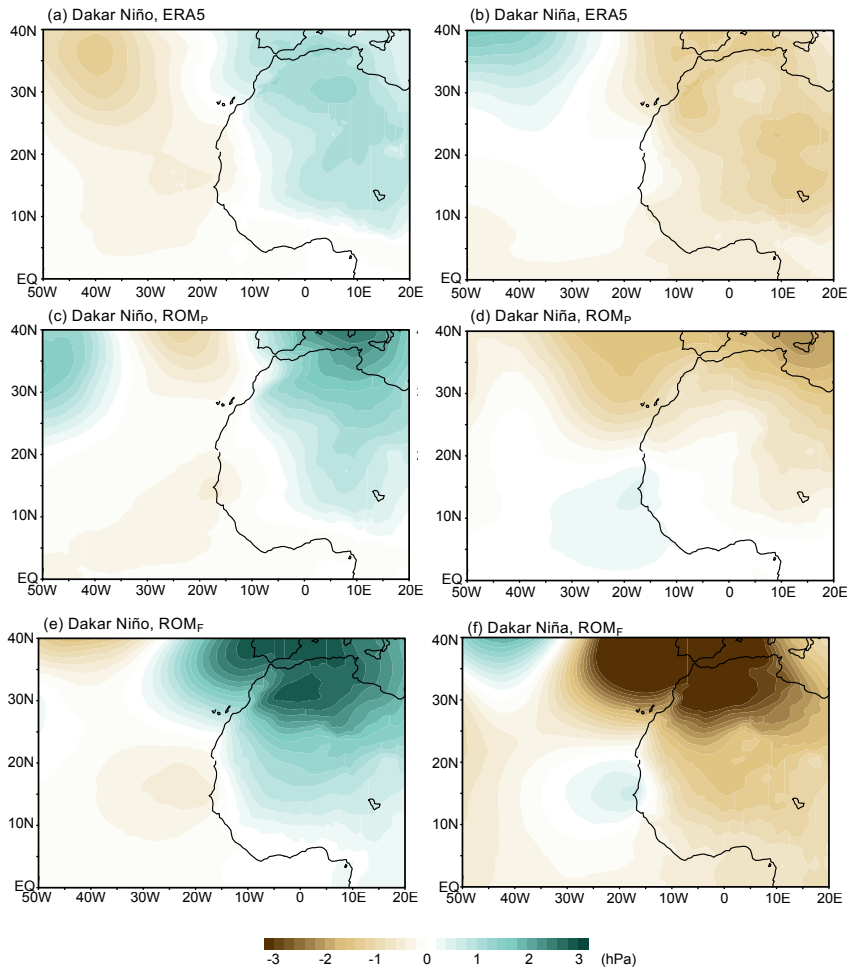
Figure 10: Same as Fig. 9 , but for sea level pressure in a wider domain.

SLP anomaly pattern that connects to the Mediterranean although the Azores high anomalies are not as clear as ERA5 (Figs. 10c and d). However, the cores of the continental SLP anomalies are located around 0 to 20°E, which is in line with ERA5. In the ROM$_F$, the continental SLP anomalies intensify as the 2m temperature anomalies are strengthened (Figs. 9e, f, 10e and f). The SLP anomaly gradient runs along the coastal region of western African and this situation is favourable for meridional surface wind anomaly for Dakar Niño (reducing equatorward wind anomaly) and Nina (increasing equatorward wind anomaly). Interestingly, the Mediterranean SLP anomalies are intensively strengthened in both cases and accordingly the Sahara SLP anomalies are stronger creating a sharper zonal SLP gradient along the western Africa coast. It is reported that the inter-annual

variability in the temperature experiences future intensification in the Mediterranean region under global warming (Giorgi and Lionello, 2008) and the Mediterranean SLP anomalies are also expected to be amplified in the future.

According to (Oettli et al., 2016), surface heat flux is responsible for generating Dakar Niño and Niña events. On the other hand, as suggested by Figs. 6, 7, 9, and 10, the meridional surface wind variability is strengthened and consequently, this can influence the ocean dynamics like vertical motion and ocean current affecting the Dakar Niño and Niña events in the future climate. To quantify this, here we examine the heat budget in the ocean mixing layer during Dakar Niño and Niña events. Following (Vijith et al., 2020), we consider the heat budget in the ocean mixing layer is estimated as follows,

$$\frac{\partial \text{SST}}{\partial t} = \langle -u\frac{\partial T}{\partial x} \rangle + \langle -v\frac{\partial T}{\partial y} \rangle + w_{OML}\frac{\Delta T}{D} + R,$$

Here, the bracket means a quantity averaged within the ocean mixing layer. D is the ocean mixing layer depth (an output of ROM). W_{OML} and ΔT denote the vertical velocity at the bottom of ocean mixing layer and the temperature difference between in the ocean mixing layer and the just below the ocean mixing layer (assuming the temperature within the ocean mixing layer is homogeneous vertically). From ROM discretized data, W_{OML} is the value at the layer just below the ocean mixing layer depth. R is a residual term that we do not examine in this study. Note that the estimation of heat budget terms is from monthly-mean data of velocity and temperature due to the limited data availability and therefore, some non-linear and transient components are missed in the heat budget.
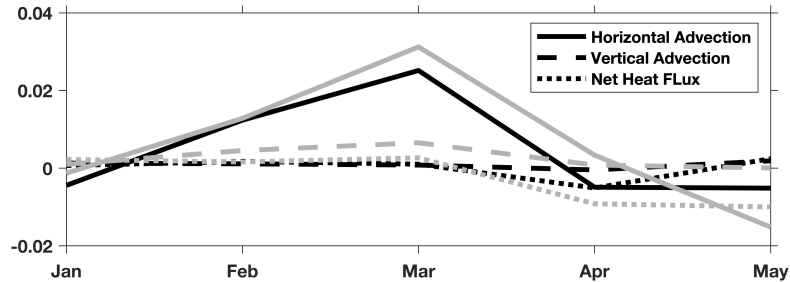
Figure 11: Monthly time series of lag-composite difference of (solid) horziontal advection, (dotted) surface net heat flux, and (dashed) vertical thermal advection between Dakar Niño and Dakar Niña events (Niño minus Niña) in (black) 1980-2010 and (grey) 2069-2099. March is lag=0. The unit is K day^{-1}.

In the present climate, the contribution of surface heat flux and vertical thermal advection is almost identical (Fig. 11), but the surface heat flux is slightly more responsible to generating warm event in February to March. However, their contribution is much smaller than horizontal advection from February to March. This large contribution of horizontal advection differs from the argument of (Oettli et al., 2016). Note that Fig. 11 shows the lag-composite difference between Dakar Niño and Niña to emphasize the anomalies during Dakar Niño (during Dakar Niña the anomalies should be opposite). After March, the surface heat flux and horizontal advection work on the warm anomalies negatively in April. Each component increases in

the future climate supporting our results of amplified Dakar Niño and Niña events. However, the horizontal and vertical thermal advection roles become almost identically important between February and March (the differences between the current and future climate 0.006K/day and 0.0057 K/day in March, respectively). This result can be explained by the strengthened alongshore wind variability. For the vertical advection, the stronger stratification at the upper layer (Fig.7e) might help the contribution of vertical advection, in particular, in Dakar Niña (Fig. 7d). The climatology of surface ocean current is slightly weakened around our focus area between ROM_P and ROM_F (the red rectangular in Fig. S5). However, the composite anomaly between Dakar Niño and Niña shows larger change in the future climate in the Dakar Index box (Fig. S5). This indicates that the stronger meridional wind variability along the coast can induce more local/regional surface ocean current change in the future than in the present climate. As (Oettli et al., 2016) suggested, the ocean mixing layer depth tends to be thinner/thicker during Dakar Niño/Niña events (see Fig. S6). This might help to increase the contribution of surface heat flux in the future climate. Because of this amplified mechanism in March, the SST anomalies can be more persisting in April in the future climate than in the present climate (Fig. 5). However, in April the thermal damping is also strengthened in the future climate and, consequently the SST anomalies suppress in May around the coast (Fig. 5).

4.2 Conclusion and future works

This study has investigated the future change of Dakar Niño variability in March employing a high-resolution regionally-coupled model, ROM with comparison between 1980-2010 and 2066-2099 under the highest emission scenario. Our model simulations show the intensification of interannual variability of SST along the northeastern tropical Atlantic and, in particular, Dakar Niña (cool SST anomaly) events tend to intensify more. This result can be consistent with (Yang et al., 2021) while they focus on the basin-scale variability in the north tropical Atlantic. In contrast, (Prigent et al., 2023) showed the weakening of the Benguela Niño under global warming. This result is discrepancy against our results, but it generates necessity of demonstrating insightful comparison between these two coastal climate modes to discuss similarity and dissimilarity of Dakar and Benguela Niños. For example, recently (Chang et al., 2023) showed the different response of eastern coast upwelling systems to climate change in northern and southern hemispheres using a set of HighResMIP models.

The stronger variability of SST in the SMFZ can be explained by the stronger local alongshore wind variability inducing a stronger horizontal and vertical thermal advection anomaly. The alongshore wind variability can be enhanced by the well-developed thermal contrast anomaly around the west African coast based on the statement of (Bakun, 1990). Moreover, we found that the corresponding Saharan sea level pressure (SLP) anomalies are extended from the Mediterranean region and the Mediterranean SLP is strengthened. In addition, the stronger stratification at 40m depth might also cause the reinforcement of the Dakar Niño/Niña variability. This stronger stratification is due to the vertically-heterogeneous warming between the surface and subsurface (e.g., Vazquez et al., 2023). The ocean surface current anomaly during Dakar Niño and Niña can be also changed by the stronger meridional wind stress in the future. Especially, the ocean current anomaly changes in the Dakar Index box.

Our discussion and argument are based on local-/regional-scale changes of surface wind and land-sea thermal/surface pressure contrast. However, as the previous studies suggest, the tropical Pacific inter-annual variability like El Niños tends to initialize the north tropical Atlantic variability including Dakar Niños via atmospheric bridge (e.g., (Lopez-Parages et al., 2020; Oettli et al., 2016), we will need to consider such teleconnection and its future change. In addition, over the north Atlantic, other dominant climate mode like North Atlantic Oscillation (NAO, e.g., (Hurrell et al., 2001) plays a crucial role in climate and weather variability over the Euro-Mediterranean region modulating the Azores high-pressure system (e.g., (Brandimarte et al., 2011; Lopez-Moreno et al., 2011). Therefore, it will be desired to explore the linkages between Dakar Niño and other climate modes like NAO and ENSO under global warming.

Code Availability

The codes used in this study can be accessed at Zonode repository, 10.5281/zenodo.10244333.

Data Availability

The data used in this study can be accessed at Zonode repository, 10.5281/zenodo.10244333.

Author Contributions

SK, VR, and WC contributed to conceptualizing the study and had discussions on the results. SK mainly performed the analyses. DSV and WC have demonstrated all the simulations used in this study. CG and MLB contributed to improving interpretation of the results and discussion. All co-authors contributed to drafting the manuscript and revising it.

Competing Interests

All co-authors declare that there is no conflict and competing interests.

Acknowledgement

SK was supported by EU Horizon 2020 TRIATLAS project (agreement number: 817578) and Giner de los Ríos 2021/22 program by University of Alcalá. RV was supported through a doctoral grant at University of Ferrara and University of Cadíz, the Spanish Ministry of Science, Innovation and Universities (I+D+I PID2021-128656OB-100) and the Plan Propio UCA 2022-23. WC and CG were funded by the Alcalá University project (PIUAH21/CC-058) and the Spanish Ministry of Science, Innovation and Universities, through grant (I+D+I PID2021-128656OB-100). DVS was supported by the Germany-Sino Joint Project (ACE, No. 2019YFE0125000 and 01LP2004A) and MHESRF scientific task № FMWE-2024-0028. MLB has received funding from the European Union's Horizon 2020 Research and Innovation Program for the project BENGUP under the Marie Skłodowska-Curie grant agreement ID 101025655. The simulations were performed at the German Climate Computing Center (DKRZ), granted by its Scientific Steering Committee (WLA) under project ID ba0987. All authors would like to express their

385 gratefulness to Prof. Noel S. Keenlyside at the University of Bergen/BCCR for his constructive comments and discussions on this work.

References

Aristegui, J., Barton, E. D., Alvarez-Salgado, X. A., Santos, A. M. P., Figueiras, F. G., Kifani, S.,
390 Hernandez-Leon, S., Mason, E., Machu, E., and Demarcq, H.: Sub-regional ecosystem variability in the Canary Current upwelling, Prog Oceanogr, 83, 33-48, 10.1016/j.pocean.2009.07.031, 2009.

Arrasate-Lopez, M., Tuset, V. M., Santana, J. I., Garcia-Mederos, A., Ayza, O., and Gonzalez, J. A.: Fishing methods for sustainable shrimp fisheries in the Canary Islands (North-West Africa), Afr J Mar Sci, 34, 331-339, 10.2989/1814232x.2012.725281, 2012.

395 Bachelery, M. L., Illig, S., and Rouault, M.: Interannual Coastal Trapped Waves in the Angola-Benguela Upwelling System and Benguela Nino and Nina events, J Marine Syst, 203, ARTN 103262 10.1016/j.jmarsys.2019.103262, 2020.

Bakun, A.: Global Climate Change and Intensification of Coastal Ocean Upwelling, Science, 247, 198-201, DOI 10.1126/science.247.4939.198, 1990.

400 Barton, E. D., Aristegui, J., Tett, P., Canton, M., Garcia-Braun, J., Hernandez-Leon, S., Nykjaer, L., Almeida, C., Almunia, J., Ballesteros, S., Basterretxea, G., Escanez, J., Garcia-Weill, L., Hernandez-Guerra, A., Lopez-Laatzen, F., Molina, R., Montero, M. F., Navarro-Perez, E., Rodriguez, J. M., van Lenning, K., Velez, H., and Wild, K.: The transition zone of the Canary Current upwelling region, Prog Oceanogr, 41, 455-504, Doi 10.1016/S0079-6611(98)00023-8, 1998.

405 Becognee, P., Almeida, C., Barrera, A., Hernandez-Guerra, A., and Hernandez-Leon, S.: Annual cycle of clupeiform larvae around Gran Canaria Island, Canary Islands, Fish Oceanogr, 15, 293-300, 10.1111/j.1365-2419.2005.00390.x, 2006.

Block, K. and Mauritsen, T.: Forcing and feedback in the MPI-ESM-LR coupled model under abruptly quadrupled CO2, J Adv Model Earth Sy, 5, 676-691, 10.1002/jame.20041, 2013.

410 Bracegirdle, T. J., Holmes, C. R., Hosking, J. S., Marshall, G. J., Osman, M., Patterson, M., and Rackow, T.: Improvements in Circumpolar Southern Hemisphere Extratropical Atmospheric Circulation in CMIP6 Compared to CMIP5, Earth Space Sci, 7, UNSP e2019EA001065 10.1029/2019EA001065, 2020.

Brandimarte, L., Di Baldassarre, G., Bruni, G., D'Odorico, P., and Montanari, A.: Relation Between the
415 North-Atlantic Oscillation and Hydroclimatic Conditions in Mediterranean Areas, Water Resour Manag, 25, 1269-1279, 10.1007/s11269-010-9742-5, 2011.

Cabos, W., de la Vara, A., Alvarez-Garcia, F. J., Sanchez, E., Sieck, K., Perez-Sanz, J. I., Limareva, N., and Sein, D. V.: Impact of ocean-atmosphere coupling on regional climate: the Iberian Peninsula case, Clim Dynam, 54, 4441-4467, 10.1007/s00382-020-05238-x, 2020.

420 Cabos, W., Sein, D. V., Pinto, J. G., Fink, A. H., Koldunov, N. V., Alvarez, F., Izquierdo, A., Keenlyside, N., and Jacob, D.: The South Atlantic Anticyclone as a key player for the representation of the tropical

Atlantic climate in coupled climate models, Clim Dynam, 48, 4051-4069, 10.1007/s00382-016-3319-9, 2017.

Chang, P., Xu, G. P., Kurian, J., Small, R. J., Danabasoglu, G., Yeager, S., Castruccio, F., Zhang, Q. Y., Rosenbloom, N., and Chapman, P.: Uncertain future of sustainable fisheries environment in eastern boundary upwelling zones under climate change, Commun Earth Environ, 4, ARTN 19 10.1038/s43247-023-00681-0, 2023.

Choudhury, B. A., Rajesh, P. V., Zahan, Y., and Goswami, B. N.: Evolution of the Indian summer monsoon rainfall simulations from CMIP3 to CMIP6 models, Clim Dynam, 58, 2637-2662, 10.1007/s00382-021-06023-0, 2022.

Colberg, F. and Reason, C. J. C.: A model study of the Angola Benguela Frontal Zone: Sensitivity to atmospheric forcing, Geophys Res Lett, 33, Artn L19608 10.1029/2006gl027463, 2006.

Cook, K. H. and Vizy, E. K.: Detection and Analysis of an Amplified Warming of the Sahara Desert, J Climate, 28, 6560-6580, 10.1175/Jcli-D-14-00230.1, 2015.

Crespo, L. R., Prigent, A., Keenlyside, N., Koseki, S., Svendsen, L., Richter, I., and Sanchez-Gomez, E.: Weakening of the Atlantic Nino variability under global warming, Nat Clim Change, 12, 822-+, 10.1038/s41558-022-01453-y, 2022.

Cropper, T. E., Hanna, E., and Bigg, G. R.: Spatial and temporal seasonal trends in coastal upwelling off Northwest Africa, 1981-2012, Deep-Sea Res Pt I, 86, 94-111, 10.1016/j.dsr.2014.01.007, 2014.

Davis, R. E., Hayden, B. P., Gay, D. A., Phillips, W. L., and Jones, G. V.: The North Atlantic subtropical anticyclone, J Climate, 10, 728-744, Doi 10.1175/1520-0442(1997)010<0728:Tnasa>2.0.Co;2, 1997.

de la Vara, A., Cabos, W., Sein, D. V., Sidorenko, D., Koldunov, N. I. V., Koseki, S., Soares, P. M. M., and Danilov, S.: On the impact of atmospheric vs oceanic resolutions on the representation of the sea surface temperature in the South Eastern Tropical Atlantic, Clim Dynam, 54, 4733-4757, 10.1007/s00382-020-05256-9, 2020.

Dee, D. P., Uppala, S. M., Simmons, A. J., Berrisford, P., Poli, P., Kobayashi, S., Andrae, U., Balmaseda, M. A., Balsamo, G., Bauer, P., Bechtold, P., Beljaars, A. C. M., van de Berg, L., Bidlot, J., Bormann, N., Delsol, C., Dragani, R., Fuentes, M., Geer, A. J., Haimberger, L., Healy, S. B., Hersbach, H., Holm, E. V., Isaksen, L., Kallberg, P., Kohler, M., Matricardi, M., McNally, A. P., Monge-Sanz, B. M., Morcrette, J. J., Park, B. K., Peubey, C., de Rosnay, P., Tavolato, C., Thepaut, J. N., and Vitart, F.: The ERA-Interim reanalysis: configuration and performance of the data assimilation system, Q J Roy Meteor Soc, 137, 553-597, 10.1002/qj.828, 2011.

Deppenmeier, A. L., Haarsma, R. J., LeSager, P., and Hazeleger, W.: The effect of vertical ocean mixing on the tropical Atlantic in a coupled global climate model, Clim Dynam, 54, 5089-5109, 10.1007/s00382-020-05270-x, 2020.

Dippe, T., Greatbatch, R. J., and Ding, H.: On the relationship between Atlantic Nio variability and ocean dynamics, Clim Dynam, 51, 597-612, 10.1007/s00382-017-3943-z, 2018.

Eyring, V., Bony, S., Meehl, G. A., Senior, C. A., Stevens, B., Stouffer, R. J., and Taylor, K. E.: Overview of
460   the Coupled Model Intercomparison Project Phase 6 (CMIP6) experimental design and organization, Geosci Model Dev, 9, 1937-1958, 10.5194/gmd-9-1937-2016, 2016.

Giorgetta, M. A., Jungclaus, J., Reick, C. H., Legutke, S., Bader, J., Bottinger, M., Brovkin, V., Crueger, T., Esch, M., Fieg, K., Glushak, K., Gayler, V., Haak, H., Hollweg, H. D., Ilyina, T., Kinne, S., Kornblueh, L., Matei, D., Mauritsen, T., Mikolajewicz, U., Mueller, W., Notz, D., Pithan, F., Raddatz, T., Rast, S., Redler,
465   R., Roeckner, E., Schmidt, H., Schnur, R., Segschneider, J., Six, K. D., Stockhause, M., Timmreck, C., Wegner, J., Widmann, H., Wieners, K. H., Claussen, M., Marotzke, J., and Stevens, B.: Climate and carbon cycle changes from 1850 to 2100 in MPI-ESM simulations for the Coupled Model Intercomparison Project phase 5, J Adv Model Earth Sy, 5, 572-597, 10.1002/jame.20038, 2013.

Giorgi, F. and Lionello, P.: Climate change projections for the Mediterranean region, Global Planet
470   Change, 63, 90-104, 10.1016/j.gloplacha.2007.09.005, 2008.

Gomez-Letona, M., Ramos, A. G., Coca, J., and Aristegui, J.: Trends in Primary Production in the Canary Current Upwelling System-A Regional Perspective Comparing Remote Sensing Models, Front Mar Sci, 4, ARTN 370
10.3389/fmars.2017.00370, 2017.

475   Good, S. A., Embury, O., Bulgin, C. E., Mittaz, J.,: ESA Sea Surface Temperature Climate Change Initiative (SST_cci): Level 4 Analysis Climate Data Record, version 2.0, 2019.

Haarsma, R. J., Roberts, M. J., Vidale, P. L., Senior, C. A., Bellucci, A., Bao, Q., Chang, P., Corti, S., Fuckar, N. S., Guemas, V., von Hardenberg, J., Hazeleger, W., Kodama, C., Koenigk, T., Leung, L. R., Lu, J., Luo, J. J., Mao, J. F., Mizielinski, M. S., Mizuta, R., Nobre, P., Satoh, M., Scoccimarro, E., Semmler, T.,
480   Small, J., and von Storch, J. S.: High Resolution Model Intercomparison Project (HighResMIP v1.0) for CMIP6, Geosci Model Dev, 9, 4185-4208, 10.5194/gmd-9-4185-2016, 2016.

Hersbach, H., Bell, B., Berrisford, P., Hirahara, S., Horanyi, A., Munoz-Sabater, J., Nicolas, J., Peubey, C., Radu, R., Schepers, D., Simmons, A., Soci, C., Abdalla, S., Abellan, X., Balsamo, G., Bechtold, P., Biavati, G., Bidlot, J., Bonavita, M., De Chiara, G., Dahlgren, P., Dee, D., Diamantakis, M., Dragani, R., Flemming,
485   J., Forbes, R., Fuentes, M., Geer, A., Haimberger, L., Healy, S., Hogan, R. J., Holm, E., Janiskova, M., Keeley, S., Laloyaux, P., Lopez, P., Lupu, C., Radnoti, G., de Rosnay, P., Rozum, I., Vamborg, F., Villaume, S., and Thepaut, J. N.: The ERA5 global reanalysis, Q J Roy Meteor Soc, 146, 1999-2049, 10.1002/qj.3803, 2020.

Hurrell, J. W., Kushnir, Y., and Visbeck, M.: Climate - The North Atlantic oscillation, Science, 291, 603-
490   605, DOI 10.1126/science.1058761, 2001.

Jacob, D.: A note to the simulation of the annual and inter-annual variability of the water budget over the Baltic Sea drainage basin, Meteorol Atmos Phys, 77, 61-73, DOI 10.1007/s007030170017, 2001.

Jungclaus, J. H., Fischer, N., Haak, H., Lohmann, K., Marotzke, J., Matei, D., Mikolajewicz, U., Notz, D., and von Storch, J. S.: Characteristics of the ocean simulations in the Max Planck Institute Ocean Model
495   (MPIOM) the ocean component of the MPI-Earth system model, J Adv Model Earth Sy, 5, 422-446, 10.1002/jame.20023, 2013.

Klenz, T., Dengler, M., and Brandt, P.: Seasonal Variability of the Mauritania Current and Hydrography at 18°N, J Geophys Res-Oceans, 123, 8122-8137, 10.1029/2018jc014264, 2018.

Koseki, S. and Koungue, R. A. I.: Regional atmospheric response to the Benguela Ninas, Int J Climatol, 41, E1483-E1497, 10.1002/joc.6782, 2021.

Koseki, S., Giordani, H., and Goubanova, K.: Frontogenesis of the Angola-Benguela Frontal Zone, Ocean Sci, 15, 83-96, 10.5194/os-15-83-2019, 2019.

Koungue, R. A. I., Rouault, M., Illig, S., Brandt, P., and Jouanno, J.: Benguela Ninos and Benguela Ninas in Forced Ocean Simulation From 1958 to 2015, J Geophys Res-Oceans, 124, 5923-5951, 10.1029/2019jc015013, 2019.

Koungue, R. A. I., Brandt, P., Luebbecke, J., Prigent, A., Martins, M. S., and Rodrigues, R. R.: The 2019 Benguela Nino, Front Mar Sci, 8, ARTN 800103
10.3389/fmars.2021.800103, 2021.

Lazaro, C., Fernandes, M. J., Santos, A. M. P., and Oliveira, P.: Seasonal and interannual variability of surface circulation in the Cape Verde region from 8 years of merged T/P and ERS-2 altimeter data, Remote Sens Environ, 98, 45-62, 10.1016/j.rse.2005.06.005, 2005.

Lopez-Moreno, J. I., Vicente-Serrano, S. M., Moran-Tejeda, E., Lorenzo-Lacruz, J., Kenawy, A., and Beniston, M.: Effects of the North Atlantic Oscillation (NAO) on combined temperature and precipitation winter modes in the Mediterranean mountains: Observed relationships and projections for the 21st century, Global Planet Change, 77, 62-76, 10.1016/j.gloplacha.2011.03.003, 2011.

Lopez-Parages, J., Auger, P. A., Rodriguez-Fonseca, B., Keenlyside, N., Gaetan, C., Rubino, A., Arisido, M. W., and Brochier, T.: El Nino as a predictor of round sardinella distribution along the northwest African coast, Prog Oceanogr, 186, ARTN 102341
10.1016/j.pocean.2020.102341, 2020.

Marsland, S. J., Haak, H., Jungclaus, J. H., Latif, M., and Roske, F.: The Max-Planck-Institute global ocean/sea ice model with orthogonal curvilinear coordinates, Ocean Model, 5, 91-127, Pii S1463-5003(02)00015-X
Doi 10.1016/S1463-5003(02)00015-X, 2003.

Martin-Rey, M. and Lazar, A.: Is the boreal spring tropical Atlantic variability a precursor of the Equatorial Mode?, Clim Dynam, 53, 2339-2353, 10.1007/s00382-019-04851-9, 2019.

Mittelstaedt, E.: The Ocean Boundary Along the Northwest African Coast - Circulation and Oceanographic Properties at the Sea-Surface, Prog Oceanogr, 26, 307-355, Doi 10.1016/0079-6611(91)90011-A, 1991.

Ndoye, S., Capet, X., Estrade, P., Sow, B., Dagorne, D., Lazar, A., Gaye, A., and Brehmer, P.: SST patterns and dynamics of the southern Senegal-Gambia upwelling center, J Geophys Res-Oceans, 119, 8315-8335, 10.1002/2014jc010242, 2014.

Oettli, P., Morioka, Y., and Yamagata, T.: A Regional Climate Mode Discovered in the North Atlantic: Dakar Nino/Nina, Sci Rep-Uk, 6, ARTN 18782
10.1038/srep18782, 2016.

535   Pardo, P. C., Padin, X. A., Gilcoto, M., Farina-Busto, L., and Perez, F. F.: Evolution of upwelling systems coupled to the long-term variability in sea surface temperature and Ekman transport, Clim Res, 48, 231-246, 10.3354/cr00989, 2011.

Pastor, M. V., Pelegri, J. L., Hernandez-Guerra, A., Font, J., Salat, J., and Emellanov, M.: Water and nutrient fluxes off Northwest Africa, Cont Shelf Res, 28, 915-936, 10.1016/j.csr.2008.01.011, 2008.

540   Perez-Hernandez, M. D., Hernandez-Guerra, A., Fraile-Nuez, E., Comas-Rodriguez, I., Benitez-Barrios, V. M., Dominguez-Yanes, J. F., Velez-Belchi, P., and De Armas, D.: The source of the Canary current in fall 2009, J Geophys Res-Oceans, 118, 2874-2891, 10.1002/jgrc.20227, 2013.

Priestley, M. D. K., Ackerley, D., Catto, J. L., Hodges, K. I., McDonald, R. E., and Lee, R. W.: An Overview of the Extratropical Storm Tracks in CMIP6 Historical Simulations, J Climate, 33, 6315-6343,
545   10.1175/Jcli-D-19-0928.1, 2020.

Prigent, A., Koungue, R. A. I., Lübbecke, J. F., Brandt, P., Harlass, J., and Latif, M.: Future weakening of southeastern tropical Atlantic Ocean interannual sea surface temperature variability in a global climate model, Clim Dynam, 10.1007/s00382-023-07007-y, 2023.

Richter, I. and Tokinaga, H.: An overview of the performance of CMIP6 models in the tropical Atlantic:
550   mean state, variability, and remote impacts, Clim Dynam, 55, 2579-2601, 10.1007/s00382-020-05409-w, 2020.

Richter, I. and Xie, S. P.: On the origin of equatorial Atlantic biases in coupled general circulation models, Clim Dynam, 31, 587-598, 10.1007/s00382-008-0364-z, 2008.

Rouault, M., Illig, S., Lubbecke, J., and Koungue, R. A. I.: Origin, development and demise of the 2010-
555   2011 Benguela Nino, J Marine Syst, 188, 39-48, 10.1016/j.jmarsys.2017.07.007, 2018.

Santana-Falcon, Y., Mason, E., and Aristegui, J.: Offshore transport of organic carbon by upwelling filaments in the Canary Current System, Prog Oceanogr, 186, ARTN 102322 10.1016/j.pocean.2020.102322, 2020.

Sein, D. V., Mikolajewicz, U., Groger, M., Fast, I., Cabos, W., Pinto, J. G., Hagemann, S., Semmler, T.,
560   Izquierdo, A., and Jacob, D.: Regionally coupled atmosphere-ocean-sea ice-marine biogeochemistry model ROM: 1. Description and validation, J Adv Model Earth Sy, 7, 268-304, 10.1002/2014ms000357, 2015.

Sein, D. V., Groger, M., Cabos, W., Alvarez-Garcia, F. J., Hagemann, S., Pinto, J. G., Izquierdo, A., de la Vara, A., Koldunov, N. V., Dvornikov, A. Y., Limareva, N., Alekseeva, E., Martinez-Lopez, B., and Jacob,
565   D.: Regionally Coupled Atmosphere-Ocean-Marine Biogeochemistry Model ROM: 2. Studying the Climate Change Signal in the North Atlantic and Europe, J Adv Model Earth Sy, 12, ARTN e2019MS001646 10.1029/2019MS001646, 2020.

Shen, M. L., Keenlyside, N., Selten, F., Wiegerinck, W., and Duane, G. S.: Dynamically combining
570   climate models to "supermodel" the tropical Pacific, Geophys Res Lett, 43, 359-366, 10.1002/2015gl066562, 2016.

Soares, P. M. M., Lima, D. C. A., Semedo, A., Cardoso, R. M., Cabos, W., and Sein, D.: The North African coastal low level wind jet: a high resolution view (vol 53, pg 1211, 2019), Clim Dynam, 53, 1231-1231, 10.1007/s00382-018-4475-x, 2019.

575 Sylla, A., Gomez, E. S., Mignot, J., and Lopez-Parages, J.: Impact of increased resolution on the representation of the Canary upwelling system in climate models, Geosci Model Dev, 15, 8245-8267, 10.5194/gmd-15-8245-2022, 2022.

Sylla, A., Mignot, J., Capet, X., and Gaye, A. T.: Weakening of the Senegalo-Mauritanian upwelling system under climate change, Clim Dynam, 53, 4447-4473, 10.1007/s00382-019-04797-y, 2019.

580 Toniazzo, T. and Koseki, S.: A Methodology for Anomaly Coupling in Climate Simulation, J Adv Model Earth Sy, 10, 2061-2079, 10.1029/2018ms001288, 2018.

Vazquez, R., Parras-Berrocal, I., Cabos, W., Sein, D. V., Mananes, R., and Izquierdo, A.: Assessment of the Canary current upwelling system in a regionally coupled climate model, Clim Dynam, 58, 69-85, 10.1007/s00382-021-05890-x, 2022.

585 Vijith, V., Vinayachandran, P. N., Webber, B. G. M., Matthews, A. J., George, J. V., Kannaujia, V. K., Lotliker, A. A., and Amol, P.: Closing the sea surface mixed layer temperature budget from in situ observations alone: Operation Advection during BoBBLE, Sci Rep-Uk, 10, ARTN 7062 10.1038/s41598-020-63320-0, 2020.

Voldoire, A., Exarchou, E., Sanchez-Gomez, E., Demissie, T., Deppenmeier, A. L., Frauen, C.,
590 Goubanova, K., Hazeleger, W., Keenlyside, N., Koseki, S., Prodhomme, C., Shonk, J., Toniazzo, T., and Traore, A. K.: Role of wind stress in driving SST biases in the Tropical Atlantic, Clim Dynam, 53, 3481-3504, 10.1007/s00382-019-04717-0, 2019.

Yang, Y., Wu, L. X., Cai, W. J., Jia, F., Ng, B., Wang, G. J., and Geng, T.: Suppressed Atlantic Nino/Nina variability under greenhouse warming, Nat Clim Change, 12, 814-+, 10.1038/s41558-022-01444-z,
595 2022.

Yang, Y., Wu, L. X., Guo, Y., Gan, B. L., Cai, W. J., Huang, G., Li, X. C., Geng, T., Jing, Z., Li, S. J., Liang, X., and Xie, S. P.: Greenhouse warming intensifies north tropical Atlantic climate variability, Sci Adv, 7, ARTN eabg9690 10.1126/sciadv.abg9690, 2021.

600 Zhou, L. M.: Desert Amplification in a Warming Climate, Sci Rep-Uk, 6, ARTN 31065 10.1038/srep31065, 2016.

Zuo, H., Balmaseda, M. A., Tietsche, S., Mogensen, K., and Mayer, M.: The ECMWF operational ensemble reanalysis-analysis system for ocean and sea ice: a description of the system and assessment, Ocean Sci, 15, 779-808, 10.5194/os-15-779-2019, 2019.

605